In-depth proteomics identifies a role for autophagy in controlling ROS-mediated endothelial permeability

Francesca Patella[1], Lisa J Neilson[1], Dimitris Athineos[1], Zahra Erami[1], Kurt Anderson[1], Karen Blyth[1], Kevin M Ryan[1] and Sara Zanivan[1,*]

[1]Cancer Research UK Beatson Institute, Glasgow G611BD, UK

*Correspondence: s.zanivan@beatson.gla.ac.uk , tel. +44(0)141 330 3971

Running Title: Autophagy controls endothelial permeability

Abstract

Endothelial cells (ECs) form the inner layer of blood vessels and physically separate the blood from the surrounding tissue. To support tissues with nutrients and oxygen, the endothelial monolayer is semipermeable. When EC permeability is altered, blood vessels are not functional and this is associated with disease. A comprehensive knowledge of the mechanisms regulating EC permeability is key in developing strategies to target this mechanism in pathologies. Here we have used an in vitro model of human umbilical vein endothelial cells mimicking the formation of a physiologically permeable vessel and performed time-resolved in-depth molecular profiling using SILAC MS-proteomics. Autophagy is induced when ECs are assembled into a physiologically permeable monolayer. By using siRNA and drug treatment to block autophagy in combination with functional assays and MS proteomics, we show that ECs require autophagy flux to maintain intracellular reactive oxygen species levels and this is required to maintain the physiological permeability of the cells.

Keywords

.

Introduction

Endothelial cells (ECs) line the inner wall of blood vessels as a semipermeable monolayer that physically separates the blood from the surrounding tissues [1]. The maintenance of endothelial cell permeability is critical to the physiological function of blood vessels in distributing oxygen and nutrients throughout the entire organism. In the mature vasculature, the endothelial monolayer is constituted of quiescent cells [2], which are tightly connected to each other through cell-cell adhesion protein complexes called tight junctions and adherens junctions [3]. The disruption of these junctions results in a leaky vasculature, which is a hallmark of diseases, such as cancer [4,5]. Several mechanisms regulating EC hyperpermeability have already been well characterized. For example, upon binding to their receptors, the vascular endothelial growth factor (VEGF) [6,7] and the pro-inflammatory factors thrombin and histamine[8,9] activate Ca^{2+}, Rho GTPase/ROCK, and myosin light chain kinase signaling pathways. Those pathways, in turn, induce the disruption of intercellular junctions between ECs. We have recently shown that EC metabolism is a key controller of vascular permeability, particularly that fatty acid oxidation is required to maintain the physiological permeability of the endothelial cells [10]. This highlights the complexity of the mechanisms regulating vascular permeability, and suggests that other pathways may play a key role in this process. To address this question, we have applied unbiased time-resolved MS-based proteomics to an *in vitro* model where endothelial cells, cultured for one week with growth factor stimulation, assemble into a monolayer [11]. This model recapitulates aspects of the formation of a physiologically permeable blood vessel.

Autophagy is a catabolic process that leads to the degradation of cellular proteins and organelles, and it is crucial to maintain cellular homeostasis. Autophagy is often induced when cells are under stress conditions triggered by stimuli such as reactive oxygen species (ROS), amino acid starvation and hypoxia. For example, autophagy can generate free amino acids and fatty acids, which are used by the cells as building blocks to survive under nutrient limitation [12]. Autophagy is a multistep process whereby targeted cytoplasmic components

are engulfed by double membrane organelles called autophagosomes [13]. The fusion of an autophagosome to a lysosome generates an autolysosome, which degrades its contents by virtue of its acidic pH and the presence of lytic enzymes [14,15]. Autophagy (ATG)-related proteins tightly regulate the autophagy process. As an example, ATG5 controls the formation of autophagosomes. Notably, ATG proteins can be targeted to inhibit autophagy [12].

Autophagy is active in ECs *in vitro* and *in vivo*, but its functional role in ECs is quite controversial. In human umbilical vein endothelial cells (HUVECs) autophagy is induced upon silencing of VEGF and this leads to cell death [16]. Conversely, autophagy promotes cell survival in response to hypoxia in bovine aortic ECs (BAECs) cultured under glucose-deprived conditions [17]. Autophagy has also been implicated in regulating vessel growth. By manipulating the expression of ATG5, it has been shown that autophagy enhances the ability of nutrient deprived BAEC to assemble in a capillary-like network when cultured on matrigel [18]. However, HUVECs silenced for ATG5 do not have any sprouting defects when embedded into a three dimensional gel [19]. In contrast, inhibition of autophagy by silencing ATG5 in HUVECs enhances their assembly into network-like structures when co-cultured with neuroblastoma cells [20]. *In vivo,* EC-specific deletion of *Atg5* or *Atg7* in mice did not affect postnatal retinal angiogenesis [21][65]. However it decreased von Willebrand factor (vWF) release upon epinephrine stimulation, with a consequent prolongation of bleeding time [21]. Finally, EC-deletion of *Atg5* in mice bearing a graft of B16-F10 melanoma cells produced tumors with smaller, more numerous and tortuous vessels [19]. Hence autophagy is necessary for the regulation of endothelial functions.

By in depth measurement of the proteomes of HUVECs cultured either sparsely or tightly confluent in the presence of nutrients and growth factors, we have discovered that autophagy levels are higher in a fully formed endothelial monolayer. We show that inhibiting autophagy in ECs, either pharmacologically or by silencing ATG5 with siRNA, impairs their permeability. Bioinformatic analysis of proteomic changes occurring upon inhibition of autophagy in ECs, predicted ROS as an upstream regulator of the measured changes.

Finally, we show that HUVECs require autophagy to control ROS levels in order to maintain their permeability.

Experimental Section

Cell culture and transfection. Human Umbilical Vein Endothelial Cells (HUVECs) isolated from 2-5 umbilical cords were pooled together and cultured in EGM-2 (Lonza, Basel, Switzerland) until passage 6 on 1% gelatin-coated dishes. Cells were nucleofected with 60 pmol of si-ATG5 (RNA-Stealth, pool three single siRNAs, Thermo Fisher Scientific) or si-NC (non-targeting siRNA, Thermo Fisher Scientific) per 10^6 cells using Amaxa nucleofector and nucleofector kit (Lonza) and experiments were performed 4 days after transfection.

SILAC labeling. To generate the EC SILAC standard, HUVECs were cultured in custom-made EGM-2 without arginine and lysine (Lonza) supplemented with $^{13}C_6^{15}N_4$ L-arginine, and $^{13}C_6^{15}N_2$ L-lysine (SILAC heavy) (Cambridge Isotope Laboratories) for 3 passages, corresponding to more than 97% of heavy aminoacid incorporation.

Cell lysis and sample preparation for proteomic analysis. Sample lysate in 2% SDS in 0.1 M Tris HCl buffer pH 7.4 was mixed with an equal protein amount (125 µg for the confluency experiment, 5 µg for the bafilomycin experiment, 65 µg for the si-ATG5 experiment) of SILAC internal standard.

For the confluency and si-ATG5 experiment, three replicates (cells cultured separately and processed on the same day) were analyzed. Proteins were trypsin (sequencing grade modified, Promega) digested using the filter-aided sample preparation protocol [22] and peptides fractionated into six fractions using pipette tip strong anion exchange separation microcolumn [23].

For the bafilomycin experiment, three replicates (cells cultured separately and processed on the same day) were analyzed. Proteins were precipitated in methanol-chloroform,

resuspended in urea buffer (8M urea, 75mM NaCl, 50mM Tris), reduced with dithiothreitol, and alkylated with iodoacetamide. Endoproteinase Lys-C (Waco) followed by trypsin were used to digest the proteins (enzyme to protein ratio = 1:50).

For the conditioned medium analysis, ECs were grown until confluence in EGM-2 medium. They were washed in PBS with Ca^{2+} and Mg^{2+} and treated or not with bafilomycin 100 nM in EGM-2 without serum. After 4 hours the supernatant was collected and spun at 4°C (300 g for 10 minutes, followed by 2,000 g for 10 minutes and 10,000 g for 30 minutes). The proteins in the supernatant were extracted as previously described [24]. Collected proteins were precipitated with methanol and chloroform, resuspended in 8 M urea buffer, reduced, alkylated and Lys-C and trypsin digested.

Peptides were desalted by using C_{18} StageTip [25] and eluted in 80% acetonitrile, 0.5% acetic acid and stored at -20 °C until analyzed at the MS.

Mass spectrometry analysis. Proteomic MS analysis was performed using a linear trap quadrupole (LTQ)-Orbitrap Elite (Thermo Fisher Scientific), operated in the high energy collision dissociation (HCD) fragmentation mode, coupled on-line with a nano-liquid chromatography (nLC) (EasynLC, Thermo Fisher Scientific) as described previously [10]. The tryptic peptides were separated on a 20 cm reverse phase column packed with 1.9 μm C_{18} resin (Dr.Maisch, GmbH, Ammerbuch-Entringen, Germany) using a flow of 200 nl/min in 90 min gradient from 5% to 25% ACN in 0.5% acetic acid. The MS spectra were acquired in the Orbitrap analyzer at a resolution of 120,000 at 400 m/z, and a target value of 10^6 charges. HCD fragmentation of the 10 most intense ions was performed using a target value of 40,000 charges which were acquired in the Orbitrap at a resolution 15,000 at 400 m/z. Data were acquired with Xcalibur software.

MS proteomic data analysis. MS data were processed using the MaxQuant computational platform [26] (version 1.3.6.0 for the cell confluency proteomes and 1.3.8.2 for the autophagy-inhibited proteomes) and searched with Andromeda search engine [27] against the human

UniProt database (release-2012 01, 88,847 entries). The 'match between runs' [26] option was enabled. An initial maximal mass deviation of 7 ppm and 20 ppm was required to search for precursor and fragment ions, respectively. Trypsin with full enzyme specificity and peptides with a minimum length of seven amino acids were selected, and two missed cleavages were allowed. Oxidation (Met) and N-acetylation were set as variable modifications, whereas Carbamidomethylation (Cys) as fixed modification. False discovery rate (FDR) of 1% was used for peptides and proteins identification. Only proteins identified with a minimum of one unique peptide and quantified with a minimum of two ratio counts were used for the analysis. Only peptides uniquely identified were used for protein quantification. The relative quantification of the peptides against their SILAC-labeled counterparts was performed by MaxQuant. Label-free quantification was performed with the label-free algorithm integrated in MaxQuant [28]. Common contaminants [26] were excluded from the analysis.

Data analysis. MS data statistical analysis and 2D analysis were performed with Perseus software [29]. Comparative pathway analysis was performed with Ingenuity® Pathway Analysis IPA®, QIAGEN Redwood City, www.qiagen.com/ingenuity .

Cell proliferation and apoptosis. To assess cell proliferation, HUVECs were incubated with EdU for 1.5 h. After harvesting and staining with Click-iT EdU kit (Invitrogen) according to manufacturer's recommendations, EdU incorporation was analyzed by FACS. To assess apoptotic cell death, Annexin V kit (Invitrogen) was used according to manufacturer's recommendations and cells were analyzed by FACS.

Immunoblot analysis. HUVECs were lysed in 2% SDS in 0.1 M Tris HCl pH 7.4 and mouse ECs in 50 mM TrisHCl, pH 7.5, 140 mM NaCl, 1% Igepal and complete protease inhibitor (Roche) buffer. Proteins were separated on 4-12% gradient NuPAGE Novex Bis-Tris gel (Life Technologies) and transferred to PVDF membranes (Millipore). The membranes were probed with the following primary antibodies: anti-ATG7 (H-300, sc-33211), anti-β tubulin (H-235, sc-9104) from Santa Cruz Biotechnology; anti-vinculin (V9131) from Sigma; anti-ATG5

(D1G9, #8540) and anti-LC3B (#2775) from Cell Signaling; anti-p62/SQSTM1 (#PM045) from MBL.

Permeability assay (Trans Endothelial Electrical Resistance, TEER). HUVECs were plated on 0.4 µm pore size polyester membrane (Corning, New York, NY) pre-coated with 1% gelatin and grown 100% confluent. STX2 electrode connected to an EVOM2 voltohmmeter (World Precision Instruments) was used to measure TEER. The background resistance measured in transwells with no cells was subtracted from the transwells with cells.

Permeability assay (FITC-dextran or FITC-albumin). HUVECs were plated and grown as for the TEER assay and treated as indicated. For the ROS scavenging experiment, the cells were pre-incubated with N-acetyl-L-cysteine (1mM, Sigma) and ascorbic acid (vitamin C, 500 µM, Sigma) for 15 minutes before treatment with 100 nM bafilomycin. FITC-dextran 40 KDa or FITC-albmin 65 KDa, 10 µM (Sigma-Aldrich), was then added in the top wells and after 30 minutes the transwells were disassembled and the fluorescence of the medium in the bottom chamber was measured by using a fluorescence plate reader.

Mice and Miles assay

The C57Bl/6 mice with endothelial-specific deletion of *Atg7* were generated by cross-breeding *Atg7$^{flox/flox}$* (kindly provided by Prof. Masaaki Komatsu) with *Cdh5* (PAC)-Cre^{ERT2} mice (kindly provided by Prof. Ralf Adams) to produce *Atg7$^{flox/+}$Cdh5*-Cre$^{+/-}$. These mice were further crossed to generate *Atg7$^{flox/flox}$Cdh5*-Cre$^{-/-}$ (used as control) or *Atg7$^{flox/flox}$Cdh5*-Cre$^{+/-}$ mice. Three mice per genotype were used to extract the lungs which were used to isolate endothelial cells. Mice were injected intraperitoneally with 2 mg of tamoxifen daily for three days and sacrificed two weeks later.

Mouse lung endothelial cells (MLECs) were isolated from lungs of 8 weeks old mice with slight modification to the protocol previously described [30]. Mice were culled by cervical dislocation and lungs placed in Opti-MEM (Life Technologies) with 20% fetal bovine serum

and antibiotics. Minced tissue was left for 45 minutes at 37ºC in pre-warmed 2mg/ml type 1 collagenase (Sigma) in Dulbecco's PBS (Sigma). The cell suspension was gently passed through a 19 gauge cannula twelve times then through a 70µm cell strainer prior to being centrifuged and the pellet re-suspended in cold PBS/0.1% bovine serum albumin. Cell suspension was incubated for 10 minutes at room temperature with Dynabeads (Dynal) pre-coated with anti-mouse CD102 (Icam-2) antibody (Pharmingen), 15 µl of beads/ml of cell suspension. After separation and washes using a magnetic separator, the cells were plated in M199 (Invitrogen) with antibiotics, 16% fetal bovine serum, 10 µg/ml heparin, 2 mM glutamine and endothelial cell growth supplement (Sigma). A second sort with the magnetic beads was performed after 3 days of culture.

The Miles assay was performed as previously described with minor modifications [31]. Briefly, 30 min before Evans blue injection, mice were intra-peritoneally injected with 100 µl of pyrilamine maleate salt (4 mg/kg body weight in 0.9% saline, Sigma-Aldrich) to inhibit histamine release. Then 200 µl of 0.5% solution of Evans blue were injected tail vein and left in the circulation for 20 min. Mice were sacrificed by terminal anesthesia. Residual Evans Blue within the blood vessels was removed by heart perfusion with PBS followed by 0.1% PFA in PBS. Lungs were excised, weighed and processed to extract the Evans blue. After 48h incubation in formamide, the Evans blue was quantified with a spectrophotometer (wavelength = 610 nm) and normalized to the weight of the lungs.

All mouse procedures were in accordance with ethical approval from University of Glasgow under the revised Animal (Scientific Procedures) Act 1986 and the EU Directive 2010/63/EU authorized through Home Office Approval (Project license number 60/4181).

Reactive oxygen species (ROS) measurement. HUVECs were incubated for 30 minutes with 3 µM CM-H_2DCFDA probe (Invitrogen), harvested and assayed by FACS. Alternatively, cells plated on gelatin-coated glass bottom dishes were incubated with the carboxy,

H$_2$DCFDA probe (Image-iT ™ LIVE Green Reactive Oxygen Species Detection Kit, Invitrogen) and imaged live according to manufacturer's recommendations.

Experimental Design and Statistical Rational.

All the proteomic analyses were performed using samples from three replicate experiments, where cells were cultured in separate dishes, and lysed and prepared for MS analysis on the same day. For the time resolved MS-proteomic analysis, in order to compare all cell conditions between them, an ANOVA test corrected for multiple testing analysis (maximum permutation-based FDR of 0.1%) was used. For the other MS-proteomic analyses, a cut-off of 2 standard deviation (SD) from the mean of the calculated SILAC ratios was used. This test was chosen because the data (SILAC ratios of ratios) followed a normal distribution, and because the distribution of the ratios was quite narrow. This allowed us to select proteins with moderate changes in levels, but consistent between replicates.

For all other analyses, for each assay, a representative experiment of at least three reproducible independent experiments is shown. As controls we used a non-targeting siRNA for silencing experiments, and vehicle for drug-treatment experiments. In the plots, bars represent mean ± standard error of the mean (S.E.M) for n = 3 technical replicates. GraphPad Prism software was used for statistical analysis. A two-tailed unpaired t-test was used to calculate p-values: * = $p < 0.05$, ** = $p < 0.01$, *** = $p < 0.001$.

Results and Discussion

Proteomic profiling of ECs reveals increased autophagy upon reaching confluency.Endothelial cells cultured sub or tightly confluent have a distinct phenotype [11,32]. Sub-confluent cells are proliferative, motile, and almost devoid of intercellular cell-cell adhesion contacts. Confluent cells stabilize cell-cell contacts and secrete extracellular matrix (ECM) components. These latter processes contribute to inhibiting cell proliferation and making ECs quiescent [33]. This condition is typical of ECs in mature and physiologically permeable vessels *in vivo*. We reasoned that a time-resolved analysis of proteomic changes

associated with the transition from sub-confluent to confluent cells would be an excellent model to identify mechanisms required for the formation and maintenance of a physiologically permeable endothelial monolayer. We performed an in-depth MS-based proteomic analysis of HUVECs (referred to as ECs) that have been cultured sub-confluent (50% confluence, sc) or that reached a tightly confluent state after 24h (tc), 4 days (4d) or 8 days (8d) culture (Figure S1A). The culture medium was changed every second day to avoid nutrient limitation. With this setup we aimed to identify mechanisms that are activated when ECs form a monolayer, from early formation to full maturation of cell-cell adhesion contacts. To accurately quantify proteomic differences among these four cultured conditions, a lysate of SILAC-labeled ECs was used as an internal standard [34] and spiked-in to each of the unlabeled samples. From three replicate experiments, we identified 7565 proteins and quantified 4591 in at least 2 of 3 replicates (Table S1). The median reproducibility between replicates was higher than 0.8 (Pearson correlation coefficient), which highlighted the reproducibility of this study. An ANOVA test corrected for multiple testing analysis (maximum permutation-based FDR of 0.1%) identified 2221 proteins with significantly regulated levels in at least one experimental condition (Table S1). Hierarchical clustering based on average Euclidean distance (based on K-mean pre-processing, with number of clusters = 5) highlighted two major clusters. These two clusters contained proteins with either lower (blue block in Figure 1A) or higher (red block in Figure 1A) levels in confluent compared with sub-confluent cells. Gene Ontology (GO) category enrichment analysis using Fisher's exact test (Figure 1B and Table S2) pinpointed the categories that the regulated proteins belonged to. Categories related to cell division (e.g. Mitosis, p-value = 2.51×10^{-6}) and DNA/RNA-related processes (e.g. rRNA processing, p-value = 2.91×10^{-17}) were enriched in proteins which were less abundant in confluent cells. This suggests that, upon reaching confluency, ECs reduced proliferation, and is in line with the fact that cell-cell contacts in primary cells induce growth arrest [35,36]. In fact, EdU incorporation analysis showed reduced proliferation of cells cultured tc compared with sc cells. Proliferation was almost abrogated in cells cultured confluent for 4-8 days (Figure 1C). Instead, categories related to extracellular matrix (ECM)

(e.g. extracellular matrix organization, p-value =1.68×10^{-4}), metabolic process (e.g. lipid metabolic process, p-value = 3.55×10^{-9}), and vesicles (e.g. vacuole organization, p-value = 4.12×10^{-4}) were enriched in the subset of proteins whose levels increased in confluent cells. It is known that ECs in mature vessels contribute to the production and secretion of ECM components [37]. However, less is known about the contribution of vesicles and metabolic pathways to these processes. The GO category "vacuole organization" was the most enriched one, and contained several lysosomal proteins (Figure 1D, and Table S2). The levels of some of these proteins increased in confluent cells after 24h and 4h culture, and all of them increased levels after 8 day culture (Figure 1D). This suggests an increased engagement of the lysosomal compartment occurs during maturation of an endothelial monolayer. It is known that lysosomes are required for autophagy to occur. Moreover, while ATG protein levels did not change upon reaching confluency, sequestosome 1/p62 (SQSTM1) was consistently downregulated in confluent cells (Table S1). SQSTM1 is a component of the autophagic machinery which accumulates in undigested autophagosomes upon autophagy inhibition [38]. We verified SQSTM1 downregulation in confluent cells by western blot analysis (Figure 1E). These observations prompted us to investigate whether autophagy was increased in confluent ECs. First we blocked the autophagic flux by treating cells with bafilomycin A1. Bafilomycin is a well-characterized drug that inhibits the vacuolar type H^+ ATPase, thus preventing lysosomal acidification and favoring the accumulation of autophagosomes [38]. Autophagosomes contain at their membrane the lipidated form of the protein LC3B (LC3BII), which can be easily detected by western blot analysis and used to quantify autophagy flux levels in total cell lysates [38]. As expected, we assessed that autophagy flux increased in ECs upon reaching confluency. Indeed, we measured higher levels of LC3BII in bafilomycin-treated confluent compared to sub-confluent ECs. Furthermore, we showed that this was independent of the time that the cells had been confluent for (Figure 1F). Next we investigated the functional role of autophagy in ECs.

Autophagy inhibition impairs EC barrier functionality.

We assessed whether autophagy had a functional role in a confluent monolayer of ECs by inhibiting it either by acute treatment (4h) with bafilomycin or by knocking down ATG5 with siRNA (Figure 2A). First we investigated the effects of autophagy inhibition on EC proliferation. ATG5-silenced cells (si-ATG5) decreased proliferation, as measured by EdU incorporation (Figure 2B), while no changes were measured in ECs treated with bafilomycin (Figure 2C). Similarly, we measured no (Figure 2D) or minor (Figure 2E) effects on EC apoptotic death. Next, we investigated the possibility that autophagy controls other EC functions. A key function of a monolayer of ECs *in vivo* is to maintain the physiological permeability of blood vessels. *In vitro*, the permeability of a monolayer of tightly confluent ECs can be measured by trans-endothelial electrical resistance (TEER) or by using FITC-labeled dextran or albumin. The first assay measures the passage of ions (high resistance = low permeability and low resistance = high permeability). The second method measures the passage of labelled 40-65 KDa macromolecules through the EC monolayer. We used both approaches and tested the effects of autophagy inhibition on EC barrier function. For this purpose, we used ECs cultured confluent for 4 days. In this condition, cells had pronounced proteomic changes (Figure 1A). Moreover, after 4 days autophagy was induced (Figure 1F), cell proliferation was strongly reduced, as well as the levels of SQSTM1 (Figure 2B). Both approaches showed that EC permeability was significantly increased upon autophagy inhibition with ATG5 siRNA (Figure 2F,H and Figure S2A) or bafilomycin treatment (Figure 2G,I and Figure S2B). We confirmed the relevance of these results *in vivo* using adult mice that were conditionally depleted for *Atg7* within endothelial cells (*Atg7^{EC}*). The effective depletion of *Atg7* in the vasculature was measured by western blot, which showed substantially reduced levels of Atg7 in mouse primary endothelial cells isolated from *Atg7^{EC}* mice (Figure 2J). Torisu et al. [21] have previously reported that *Atg7^{EC}* mice have no clear vascular phenotypes. However, the functionality of the vasculature was not assessed in their study. Similar to Torisu et al., we could not observe any obvious phenotype in the lung vasculature of the *Atg7^{EC}* mice (not shown). Moreover, we could not measure any defects in angiogenesis, by using an *ex vivo* aortic ring assay, where the sprouting of endothelial cells

from explanted mouse aortas was induced with VEGF (not shown). However, when we assessed the functionality of the blood vessels in the lungs, we measured a striking difference, because significantly more Evans blue leaked out from the lung vasculature of $Atg7^{EC}$ mice compared with control mice (Figure 2K). Hence, autophagy is required to maintain physiological vascular barrier functionality.

Acute and long-term inhibition of autophagy with bafilomycin or si-ATG5 alters levels of proteins involved in cell motility, matrix organization and morphogenesis.

Next, we identified the molecular mechanism(s) that require a controlled autophagic flux in ECs. We used SILAC spike-in proteomics and measured proteomic changes occurring in ECs upon autophagy inhibition (Figure S1B). First we investigated the effects of acute autophagy inhibition upon 4h treatment with bafilomycin (Figure 3A and Table S3). In triplicate experiments, we identified 3888 proteins and quantified 1970 of them with a median reproducibility between replicates of 0.751 (Pearson correlation coefficient). Among the quantified proteins, 125 were up-regulated and 87 down-regulated, based on a cut-off of 2 standard deviation (SD) from the mean of the SILAC ratios (Table S3). The most upregulated protein was SQSTM1, which provided a positive control for our experimental setup. Furthermore, palmitoyl-protein thioesterase 1 (PPT1), cathepsins (CTS) B, CTSA and CTSZ, and tripeptidyl-peptidase 1(TPP1) were among the most down-regulated proteins. Such decreased amounts of lytic enzymes are typical in cells with lysosomal dysfunctions because enzymes are released in the extracellular environment [39]. Accordingly, label-free MS analysis of EC conditioned medium identified a strong accumulation of lytic enzymes in bafilomycin-treated cells (Table S4). Another protein up-regulated upon bafilomycin treatment was amyloid beta A4 protein (APP). APP is an integral membrane protein overexpressed in the endothelium of atherosclerotic and Alzheimer disease tissues and is involved in monocytic cell adhesion [40]. Interestingly, APP overexpression has been shown to promote blood-brain barrier hyperpermeability and angiogenesis [41], and endothelial dysfunction caused by APP-induced oxidative stress [42]. Next, we measured the proteomic

changes occurring by prolonged autophagy inhibition upon ATG5 knockdown in ECs. Also in this case we used a SILAC spike-in approach. In triplicate experiments with a median reproducibility between replicates of 0.882 (Pearson correlation coefficient) we identified 6807 proteins of which 5333 were quantified (Figure 3B and Table S5). Among these, 128 increased while 122 decreased levels in si-ATG5 cells based on a 2 SD cut-off from the mean SILAC ratio. Transgelin (TAGLN), transforming growth factor beta 2 (TGFB2), retinal dehydrogenase 1 (ALDH1A1) and prostaglandin G/H synthase 2 (PTGS2) were among the most up-regulated, and UHRF1-binding protein 1 (UHRF1BP1), inositol-pentakisphospate 2-kinase (IPPK), dimethyladenosine transferase 1 (TFB1M) were among the most down-regulated proteins (Table S5). A two dimension (2D) category enrichment analysis [29] revealed that most of the categories that the regulated proteins belonged to were the same, whether autophagy was inhibited with bafilomycin or si-ATG5 (Figure 3C and Table S6). In particular, the GO categories "ECM organization", "locomotion", "cell morphogenesis" and "anatomical structure formation" were enriched in the up-regulated proteins. Categories related to chromatin organization and RNA metabolic processes were enriched in the down-regulated ones. When we compared the list of regulated proteins in EC autophagy-inhibited upon drug treatment or knockdown, we identified 4 proteins commonly up-regulated (Figure 3D-E). Among those there was RHOB, a member of the Rho GTPase proteins, which are key regulators of actin dependent processes [43]. Rho GTPases have been shown to be responsible for thrombin-induced endothelial hyperpermeability in HUVECs by promoting actomyosin contractility through myosin light chain (MLC) phosphorylation [44] [45,46]. The small overlap of proteins commonly regulated between the two experimental setups may be due to several reasons: 1) autophagy was blocked at different points of the autophagic flux; 2) the different duration and extent of autophagy inhibition (several days for the siRNA, with some residual ATG5 protein; hours for the bafilomycin treatment); 3) bafilomycin affects endosomal and lysosomal functions, not only autophagy. However, despite the fact that few proteins were commonly regulated, the inhibition of autophagy with bafilomycin or ATG5

knockdown resulted in a similar EC phenotype (Figure 2A-I) and cellular function alterations (Figure 3C-D). Hence we sought the presence of common upstream regulators.

Pathway analysis predicts oxidative stress being induced upon autophagy inhibition.

We used Ingenuity Pathway Analysis (IPA) to predict the upstream drivers of the proteomic alterations upon autophagy inhibition with bafilomyicin and si-ATG5. This comparative analysis identified TGFB1, interleukin 1B (IL1B), p53 (TP53) and hydrogen peroxide, which is a major mediator of oxidative stress [47], as the most likely regulators (Figure 4A-C). All of these stimuli control, or are regulated by, autophagy [48] [49] [50]. RHOB was upregulated upon autophagy inhibition with bafilomycin and siATG5 (Figure 3D). Since RHOB is highly expressed in response to oxidative stress and increases the permeability of human pulmonary endothelial cells [51-55] we hypothesized oxidative stress as a possible driver of EC alterations induced upon autophagy inhibition. We assessed oxidative stress in autophagy-inhibited ECs by means of quantifying reactive oxygen species (ROS) with a fluorescent probe. This assay revealed a pronounced increase in ROS in bafilomycin-treated (Figure 4D) and si-ATG5 (Figure 4E) ECs compared to controls. Of note, autophagy inhibition in BAECs has been reported to reduce ROS levels [18]. This contrasting result may be due to the fact that the authors induced autophagy by serum-starving the cells, while in our work autophagy was triggered by cell-cell contact. Moreover, here we have used probes for detection of general intracellular ROS (CM-H_2DCFDA and carboxy,H_2DCFDA), while Du et al. used a probe (DHE) that specifically detects superoxide species. Further studies are therefore required to investigate the source of ROS generated upon autophagy inhibition and the link between autophagy inhibition and RHOB-dependent permeability. It is well-established that autophagy is induced by ROS to decrease oxidative stress and protect cells from damage. Our work shows that ECs additionally require autophagy to maintain ROS levels, and this corroborates the concept that a dynamic crosstalk exists between ROS and autophagy [56-58].

ROS induced by inhibition of autophagy impair EC barrier functionality.

ROS can promote endothelial hyperpermeability [59]. Therefore, we determined whether the increase in ROS upon autophagy inhibition was responsible for the impaired EC barrier functionality (Figure 2F-I). We treated ECs with bafilomycin and scavenged ROS with N-acetyl-L-cysteine (NAC) and ascorbic acid (vitamin C). Firstly, NAC and ascorbic acid were able to reduce bafilomycin-induced ROS in confluent ECs (Figure 4F). Then, we measured EC permeability by means of FITC-dextran and FITC-albumin. ROS scavengers partially restored the permeability of a monolayer of bafilomycin-treated ECs to the levels of control cells (Figure 4G and Figure S2C). This proves that oxidative stress drives the impaired barrier functionality of autophagy-inhibited ECs. Hence, we uncovered that autophagy maintains EC barrier function *in vitro* and *in vivo*. Moreover, we showed that this occurs, at least in part, through the control of ROS levels. Interestingly, Torisu et al. [21] have recently shown that mice knocked-out for *Atg7* in endothelial cells have defects in maturation and secretion of vWF, when stimulated with epinephrine. Since oxidoreductase reactions are necessary for vWF maturation [60,61] and vWF oxidation can block its proteolysis and secretion [62,63], it is tempting to speculate that autophagy controls the redox status of ECs also *in vivo*.

Conclusions

In conclusion, in this work we have used in depth quantitative proteomics and an *in vitro* model of human primary endothelial cells mimicking the formation of a stable, mature vessel, when in the presence of nutrients. We discovered that autophagy controls endothelial permeability *in vitro* and vascular permeability *in vivo*. Moreover we have unraveled part of the mechanisms behind this process and showed that ECs need autophagy to maintain their redox balance, and that this is required to maintain endothelial permeability *in vitro*. Hence, our work opens new windows to study autophagy-regulated ROS functions in blood vessels in physiology and diseases.

References

1. Sumpio, B.E., Riley, J.T. & Dardik, A. Cells in focus: endothelial cell. *The international journal of biochemistry & cell biology* **34**, 1508-1512 (2002).
2. Hobson, B. & Denekamp, J. Endothelial proliferation in tumours and normal tissues: continuous labelling studies. *British journal of cancer* **49**, 405-413 (1984).
3. Bazzoni, G. & Dejana, E. Endothelial cell-to-cell junctions: molecular organization and role in vascular homeostasis. *Physiological reviews* **84**, 869-901 (2004).
4. Carmeliet, P. Angiogenesis in life, disease and medicine. *Nature* **438**, 932-936 (2005).
5. Dudley, A.C. Tumor endothelial cells. *Cold Spring Harbor perspectives in medicine* **2**, a006536 (2012).
6. Ferrara, N. VEGF and the quest for tumour angiogenesis factors. *Nat Rev Cancer* **2**, 795-803 (2002).
7. Bates, D.O. Vascular endothelial growth factors and vascular permeability. *Cardiovascular research* **87**, 262-271 (2010).
8. Siller-Matula, J.M., Schwameis, M., Blann, A., Mannhalter, C. & Jilma, B. Thrombin as a multi-functional enzyme. Focus on in vitro and in vivo effects. *Thromb Haemost* **106**, 1020-1033 (2011).
9. Komarova, Y. & Malik, A.B. Regulation of endothelial permeability via paracellular and transcellular transport pathways. *Annual review of physiology* **72**, 463-493 (2010).
10. Patella, F.*, et al.* Proteomics-based metabolic modeling reveals that fatty acid oxidation (FAO) controls endothelial cell (EC) permeability. *Molecular & cellular proteomics : MCP* **14**, 621-634 (2015).
11. Dejana, E. Endothelial cell-cell junctions: happy together. *Nature reviews. Molecular cell biology* **5**, 261-270 (2004).
12. Yang, Z. & Klionsky, D.J. Mammalian autophagy: core molecular machinery and signaling regulation. *Current opinion in cell biology* **22**, 124-131 (2010).
13. Lamb, C.A., Yoshimori, T. & Tooze, S.A. The autophagosome: origins unknown, biogenesis complex. *Nature reviews. Molecular cell biology* **14**, 759-774 (2013).
14. Settembre, C., Fraldi, A., Medina, D.L. & Ballabio, A. Signals from the lysosome: a control centre for cellular clearance and energy metabolism. *Nature reviews. Molecular cell biology* **14**, 283-296 (2013).
15. Shen, H.M. & Mizushima, N. At the end of the autophagic road: an emerging understanding of lysosomal functions in autophagy. *Trends in biochemical sciences* **39**, 61-71 (2014).
16. Domigan, C.K.*, et al.* Autocrine VEGF maintains endothelial survival through regulation of metabolism and autophagy. *Journal of cell science* **128**, 2236-2248 (2015).
17. Wang, Q., Liang, B., Shirwany, N.A. & Zou, M.H. 2-Deoxy-D-glucose treatment of endothelial cells induces autophagy by reactive oxygen species-mediated activation of the AMP-activated protein kinase. *PloS one* **6**, e17234 (2011).
18. Du, J.*, et al.* Role of autophagy in angiogenesis in aortic endothelial cells. *American journal of physiology. Cell physiology* **302**, C383-391 (2012).
19. Maes, H.*, et al.* Tumor vessel normalization by chloroquine independent of autophagy. *Cancer cell* **26**, 190-206 (2014).
20. Kim, K.W., Paul, P., Qiao, J. & Chung, D.H. Autophagy mediates paracrine regulation of vascular endothelial cells. *Laboratory investigation; a journal of technical methods and pathology* **93**, 639-645 (2013).
21. Torisu, T.*, et al.* Autophagy regulates endothelial cell processing, maturation and secretion of von Willebrand factor. *Nature medicine* **19**, 1281-1287 (2013).
22. Wisniewski, J.R., Zougman, A., Nagaraj, N. & Mann, M. Universal sample preparation method for proteome analysis. *Nature methods* **6**, 359-362 (2009).

23.   Wisniewski, J.R., Zougman, A. & Mann, M. Combination of FASP and StageTip-based fractionation allows in-depth analysis of the hippocampal membrane proteome. *Journal of proteome research* **8**, 5674-5678 (2009).

24.   van den Biggelaar, M*., et al.* Quantitative phosphoproteomics unveils temporal dynamics of thrombin signaling in human endothelial cells. *Blood* **123**, e22-36 (2014).

25.   Rappsilber, J., Ishihama, Y. & Mann, M. Stop and go extraction tips for matrix-assisted laser desorption/ionization, nanoelectrospray, and LC/MS sample pretreatment in proteomics. *Analytical chemistry* **75**, 663-670 (2003).

26.   Cox, J. & Mann, M. MaxQuant enables high peptide identification rates, individualized p.p.b.-range mass accuracies and proteome-wide protein quantification. *Nature biotechnology* **26**, 1367-1372 (2008).

27.   Cox, J*., et al.* Andromeda: a peptide search engine integrated into the MaxQuant environment. *Journal of proteome research* **10**, 1794-1805 (2011).

28.   Wisniewski, J.R., Hein, M.Y., Cox, J. & Mann, M. A "proteomic ruler" for protein copy number and concentration estimation without spike-in standards. *Molecular & cellular proteomics : MCP* **13**, 3497-3506 (2014).

29.   Cox, J. & Mann, M. 1D and 2D annotation enrichment: a statistical method integrating quantitative proteomics with complementary high-throughput data. *BMC bioinformatics* **13 Suppl 16**, S12 (2012).

30.   Lim, Y.C. & Luscinskas, F.W. Isolation and culture of murine heart and lung endothelial cells for in vitro model systems. *Methods in molecular biology* **341**, 141-154 (2006).

31.   Sun, Z*., et al.* VEGFR2 induces c-Src signaling and vascular permeability in vivo via the adaptor protein TSAd. *J Exp Med* **209**, 1363-1377 (2012).

32.   Lampugnani, M.G*., et al.* Cell confluence regulates tyrosine phosphorylation of adherens junction components in endothelial cells. *Journal of cell science* **110 (Pt 17)**, 2065-2077 (1997).

33.   Choi, H.J*., et al.* Yes-associated protein regulates endothelial cell contact-mediated expression of angiopoietin-2. *Nature communications* **6**, 6943 (2015).

34.   Geiger, T*., et al.* Use of stable isotope labeling by amino acids in cell culture as a spike-in standard in quantitative proteomics. *Nature protocols* **6**, 147-157 (2011).

35.   Chassot, A.A*., et al.* Confluence-induced cell cycle exit involves pre-mitotic CDK inhibition by p27(Kip1) and cyclin D1 downregulation. *Cell cycle* **7**, 2038-2046 (2008).

36.   Leontieva, O.V., Demidenko, Z.N. & Blagosklonny, M.V. Contact inhibition and high cell density deactivate the mammalian target of rapamycin pathway, thus suppressing the senescence program. *Proceedings of the National Academy of Sciences of the United States of America* **111**, 8832-8837 (2014).

37.   Davis, G.E. & Senger, D.R. Endothelial extracellular matrix: biosynthesis, remodeling, and functions during vascular morphogenesis and neovessel stabilization. *Circulation research* **97**, 1093-1107 (2005).

38.   Klionsky, D.J*., et al.* Guidelines for the use and interpretation of assays for monitoring autophagy in higher eukaryotes. *Autophagy* **4**, 151-175 (2008).

39.   Nemazanyy, I*., et al.* Defects of Vps15 in skeletal muscles lead to autophagic vacuolar myopathy and lysosomal disease. *EMBO molecular medicine* **5**, 870-890 (2013).

40.   Austin, S.A. & Combs, C.K. Amyloid precursor protein mediates monocyte adhesion in AD tissue and apoE(-)/(-) mice. *Neurobiology of aging* **31**, 1854-1866 (2010).

41.   Biron, K.E., Dickstein, D.L., Gopaul, R. & Jefferies, W.A. Amyloid triggers extensive cerebral angiogenesis causing blood brain barrier permeability and hypervascularity in Alzheimer's disease. *PloS one* **6**, e23789 (2011).

42.   Iadecola, C*., et al.* SOD1 rescues cerebral endothelial dysfunction in mice overexpressing amyloid precursor protein. *Nature neuroscience* **2**, 157-161 (1999).

43. van Nieuw Amerongen, G.P. & van Hinsbergh, V.W. Cytoskeletal effects of rho-like small guanine nucleotide-binding proteins in the vascular system. *Arteriosclerosis, thrombosis, and vascular biology* **21**, 300-311 (2001).

44. Essler, M.*, et al.* Thrombin inactivates myosin light chain phosphatase via Rho and its target Rho kinase in human endothelial cells. *The Journal of biological chemistry* **273**, 21867-21874 (1998).

45. van Nieuw Amerongen, G.P., Draijer, R., Vermeer, M.A. & van Hinsbergh, V.W. Transient and prolonged increase in endothelial permeability induced by histamine and thrombin: role of protein kinases, calcium, and RhoA. *Circulation research* **83**, 1115-1123 (1998).

46. Venkatesh, D.*, et al.* RhoA-mediated signaling in Notch-induced senescence-like growth arrest and endothelial barrier dysfunction. *Arteriosclerosis, thrombosis, and vascular biology* **31**, 876-882 (2011).

47. Breton-Romero, R. & Lamas, S. Hydrogen peroxide signaling in vascular endothelial cells. *Redox biology* **2**, 529-534 (2014).

48. Lee, J., Giordano, S. & Zhang, J. Autophagy, mitochondria and oxidative stress: cross-talk and redox signalling. *The Biochemical journal* **441**, 523-540 (2012).

49. Suzuki, H.I., Kiyono, K. & Miyazono, K. Regulation of autophagy by transforming growth factor-beta (TGF-beta) signaling. *Autophagy* **6**, 645-647 (2010).

50. Lee, J.*, et al.* Autophagy suppresses interleukin-1beta (IL-1beta) signaling by activation of p62 degradation via lysosomal and proteasomal pathways. *The Journal of biological chemistry* **287**, 4033-4040 (2012).

51. Wojciak-Stothard, B.*, et al.* Role of RhoB in the regulation of pulmonary endothelial and smooth muscle cell responses to hypoxia. *Circulation research* **110**, 1423-1434 (2012).

52. Kajimoto, H.*, et al.* Oxygen activates the Rho/Rho-kinase pathway and induces RhoB and ROCK-1 expression in human and rabbit ductus arteriosus by increasing mitochondria-derived reactive oxygen species: a newly recognized mechanism for sustaining ductal constriction. *Circulation* **115**, 1777-1788 (2007).

53. Vasilaki, E.*, et al.* Transcriptional regulation of the small GTPase RhoB gene by TGF{beta}-induced signaling pathways. *FASEB journal : official publication of the Federation of American Societies for Experimental Biology* **24**, 891-905 (2010).

54. Evans, M.J., Lai, K., Shaw, L.J., Harnish, D.C. & Chadwick, C.C. Estrogen receptor alpha inhibits IL-1beta induction of gene expression in the mouse liver. *Endocrinology* **143**, 2559-2570 (2002).

55. Boiko, A.D.*, et al.* A systematic search for downstream mediators of tumor suppressor function of p53 reveals a major role of BTG2 in suppression of Ras-induced transformation. *Genes & development* **20**, 236-252 (2006).

56. Lau, A.*, et al.* A noncanonical mechanism of Nrf2 activation by autophagy deficiency: direct interaction between Keap1 and p62. *Molecular and cellular biology* **30**, 3275-3285 (2010).

57. Filomeni, G., De Zio, D. & Cecconi, F. Oxidative stress and autophagy: the clash between damage and metabolic needs. *Cell death and differentiation* **22**, 377-388 (2015).

58. Komatsu, M.*, et al.* The selective autophagy substrate p62 activates the stress responsive transcription factor Nrf2 through inactivation of Keap1. *Nature cell biology* **12**, 213-223 (2010).

59. Mehta, D. & Malik, A.B. Signaling mechanisms regulating endothelial permeability. *Physiological reviews* **86**, 279-367 (2006).

60. Metcalf, D.J., Nightingale, T.D., Zenner, H.L., Lui-Roberts, W.W. & Cutler, D.F. Formation and function of Weibel-Palade bodies. *Journal of cell science* **121**, 19-27 (2008).

61. Shapiro, S.E.*, et al.* The von Willebrand factor predicted unpaired cysteines are essential for secretion. *J Thromb Haemost* **12**, 246-254 (2014).

62. Chen, J.*, et al.* Oxidative modification of von Willebrand factor by neutrophil oxidants inhibits its cleavage by ADAMTS13. *Blood* **115**, 706-712 (2010).

63.   Lancellotti, S*., et al.* Formation of methionine sulfoxide by peroxynitrite at position 1606 of von Willebrand factor inhibits its cleavage by ADAMTS-13: A new prothrombotic mechanism in diseases associated with oxidative stress. *Free radical biology & medicine* **48**, 446-456 (2010).

64.   Vizcaino, J.A*., et al.* The PRoteomics IDEntifications (PRIDE) database and associated tools: status in 2013. *Nucleic acids research* **41**, D1063-1069 (2013).

Acknowledgments

Conflict of Interest Disclosure

The authors declare no competing financial interest.

Figures and Tables

Figure 1. Proteomic profiling reveals increase autophagy in confluent HUVECs. (A) Heat map and hierarchical clustering calculated on average Euclidean distance. The columns represent 4 different confluency states of ECs: plated sub confluent and grown for 24h (sub-confluent, sc), 4 days (confluent, 4d), or 8 days (confluent 8d) or plated at high density and grown for 24h (tightly confluent, tc). The blocks on the left highlight group of proteins increasing (in red) or decreasing (in blue) their levels upon reaching confluency. (B)

Scatter plot showing the GO biological processes (GOBP) categories enriched (Enrichment factor>1) or de-enriched (Enrichment factor <1) in the red cluster compared to the blue ones, based on Fisher's exact test analysis. Enriched categories refer to proteins whose level increased when cells reached confluency (red block in (A)). GOBP categories with Enrichment factor<1 are those enriched in proteins decreasing their level when cells reached confluency. (C) Proliferation of ECs when cultured at different confluency, as measured by EdU incorporation. (D) SILAC ratio, relative to sc cells, of lysosomal proteins that belong to the GO category "vacuole organization", which was found enriched among proteins upregulated upon confluency (B). Bars = mean +/- SEM (n = three experiments performed with cells cultured separately and processed for MS analysis on the same day). (E-F) Western blotting for p62 (E) and LC3BII (F) showing increased autophagy upon confluency. Bafilomycin was used to mark the presence of autophagy flux by blocking the autophagic degradation of LC3BII and p62. TUBB = β-tubulin, VINC=vinculin which were used as loading controls.

Figure 2. Autophagy inhibition impairs the functionality of a HUVEC monolayer. (A) Western blotting for ATG5 showing the efficiency of the silencing and levels of reduced autophagy (LC3B) in HUVECs transfected with siRNA. Quantification of ATG5 is relative to TUBB (based on LiCOR software). Bars = mean +/- SD (n = 3 independent transfections). TUBB = β-tubulin, which was used as loading control. (B-C) EC proliferation upon ATG5 siRNA (B) or 4h treatment with 100 nM bafilomycin (C), measured by EdU incorporation. (D-E) Cell death of ECs upon ATG5 knock-down (D) or bafilomycin treatment (E), measured by Annexin V and PI staining. Apoptotic cells are the Annexin V positive. (F-I) Endothelial cell barrier permeability measured by trans-endothelial electrical resistance (TEER) upon ATG5 siRNA (F) or bafilomycin treatment (G) and measured by FITC-dextran permeability upon ATG5 siRNA (H, data from 4 combined experiments) or bafilomycin treatment (I). (J) Western blotting for Atg7 showing the efficiency of *Atg7* depletion in endothelial cells isolated from tamoxifen-treated *Atg7^flox/flox^Cdh5*-Cre^+/−^ (Atg7 fl/fl) and *Atg7^flox/flox^Cdh5*-Cre^−/−^ (used as

control, Ct). Vcl = Vinculin was used as loading control. (K) Quantification of the Evans Blue injected in the vasculature and that leaked out from the blood vessels of the lungs of tamoxifen-treated *Atg7$^{flox/flox}$Cdh5*-Cre$^{+/-}$ (Atg7 fl/fl) and *Atg7$^{flox/flox}$Cdh5*-Cre$^{-/-}$ (Ct). n = 5 mice from two independent experiments.

Figure 3. Proteomics of autophagy-inhibited HUVECs. (A) Top 15 proteins with increased (top) and decreased (bottom) levels upon bafilomycin treatment (4h, 100nM). (B) Top 15 proteins with increased (top) and decreased (bottom) levels upon ATG5 siRNA. (C) Two dimension (2D) category (Gene Ontology) enrichment analysis highlighting the presence of several categories similarly enriched (red dots) and de-enriched (blue dots) when autophagy was inhibited with bafilomycin or si-ATG5. X and y axis represent the normalized averaged regulation (based on the measured SILAC ratio) of the proteins belonging to the indicated category [29]. (D) Venn diagram of proteins increasing (UP) or decreasing (DOWN) their levels in the bafilomycin and si-ATG5 experiment. (E) Proteins commonly up-regulated upon bafilomycin treatment and si-ATG5.

Figure 4. Increased ROS caused by autophagy inhibition are partially responsible for increase in endothelial barrier permeability. (A) Predicted upstream regulators in response to autophagy inhibition by si-ATG5 or bafilomyicin treatment (calculated by IPA). (B-C) Hydrogen peroxide targets found regulated upon si-ATG5 (B) or bafilomycin (C). Red = upregulated, green = downregulated, orange arrow = leads to activation, blue arrow = leads to inhibition, grey arrow = effect not predicted, yellow arrow = finding inconsistent with state of downstream molecule. (D-E) Reactive oxygen species (ROS) measurement in live cells upon autophagy inhibition by si-ATG5 (D) or bafilomycin (E). (F) Total cellular ROS measurements showing that increased ROS due to autophagy inhibition in HUVECs with bafilomycin are diminished by treating cells with the anti-oxidants N-acetyl-L-cysteine (NAC) and ascorbic acid (vitamin C). (G) Endothelial cell barrier permeability measured by FITC-dextran permeability shows that increased HUVEC barrier permeability due to autophagy blockade by bafilomycin is rescued by scavenging the ROS with NAC and vitamin C.

Supporting Information

Figures and Tables

Table S1. Proteins identified and quantified in HUVECs (total lysate) forming a tightly confluent monolayer.

Table S2. Gene Ontology (GO) category enrichment analysis of proteins regulated when HUVECs form a tightly confluent monolayer

Table S3. Proteins identified and quantified in HUVECs (total lysate) cultured confluent for 4 days upon 4h bafilomycin treatment.

Table S4. Proteins identified and quantified in HUVECs (serum-free conditioned medium) cultured confluent for 4 days upon 4h bafilomycin treatment.

Table S5. Proteins identified and quantified in HUVECs (total lysate) silenced for ATG5.

Table S6. Two dimension (2D) Gene Ontology (GO) category enrichment analysis upon autophagy inhibition with si-ATG5 or bafilomycin.

Figure S1. Proteomic analyses.

Figure S2. Autophagy inhibition increases the permeability of EC monolayer.

A

B

C

EdU incorporation

D

Lysosomal proteins

E

F

Patella et al. Figure 3
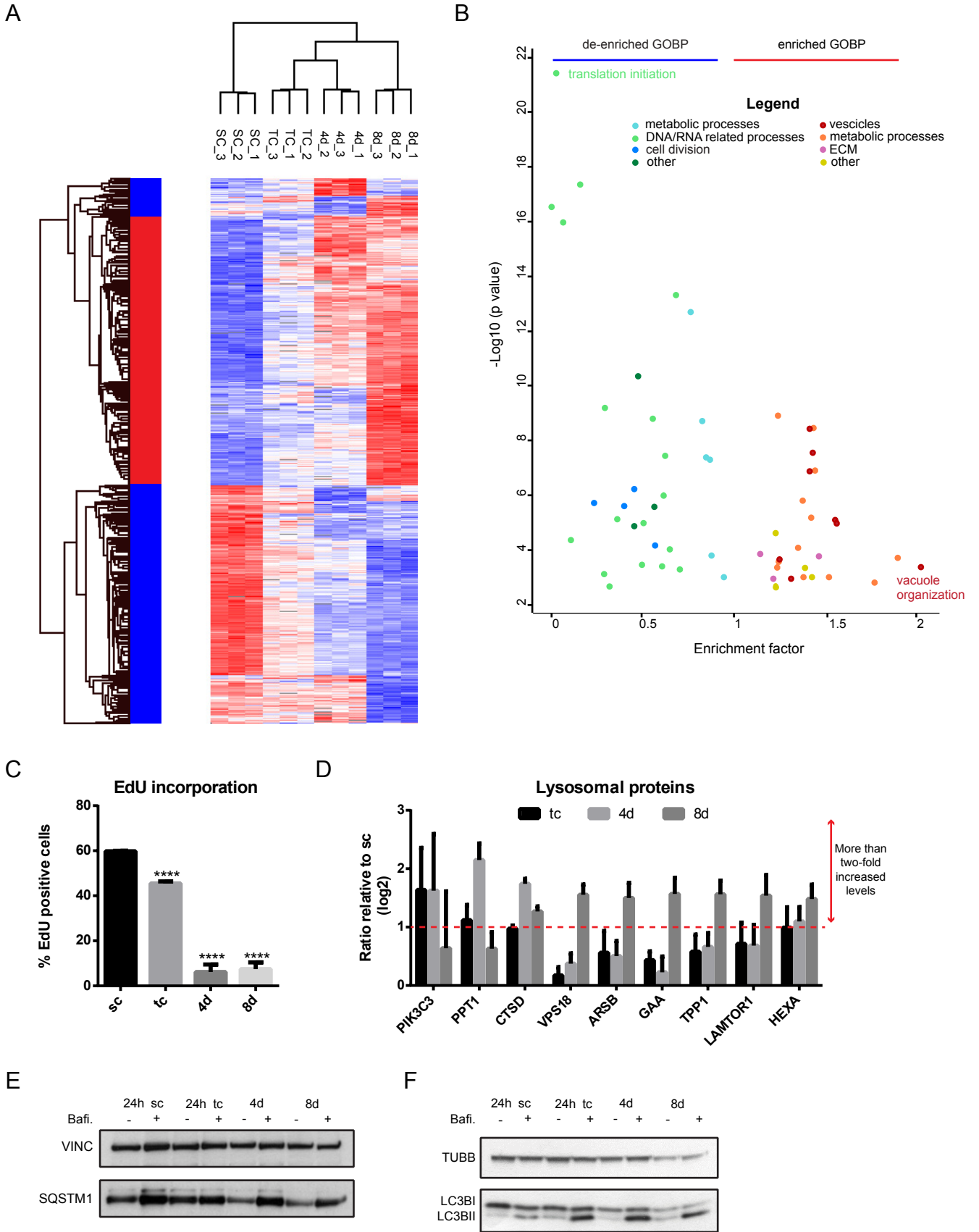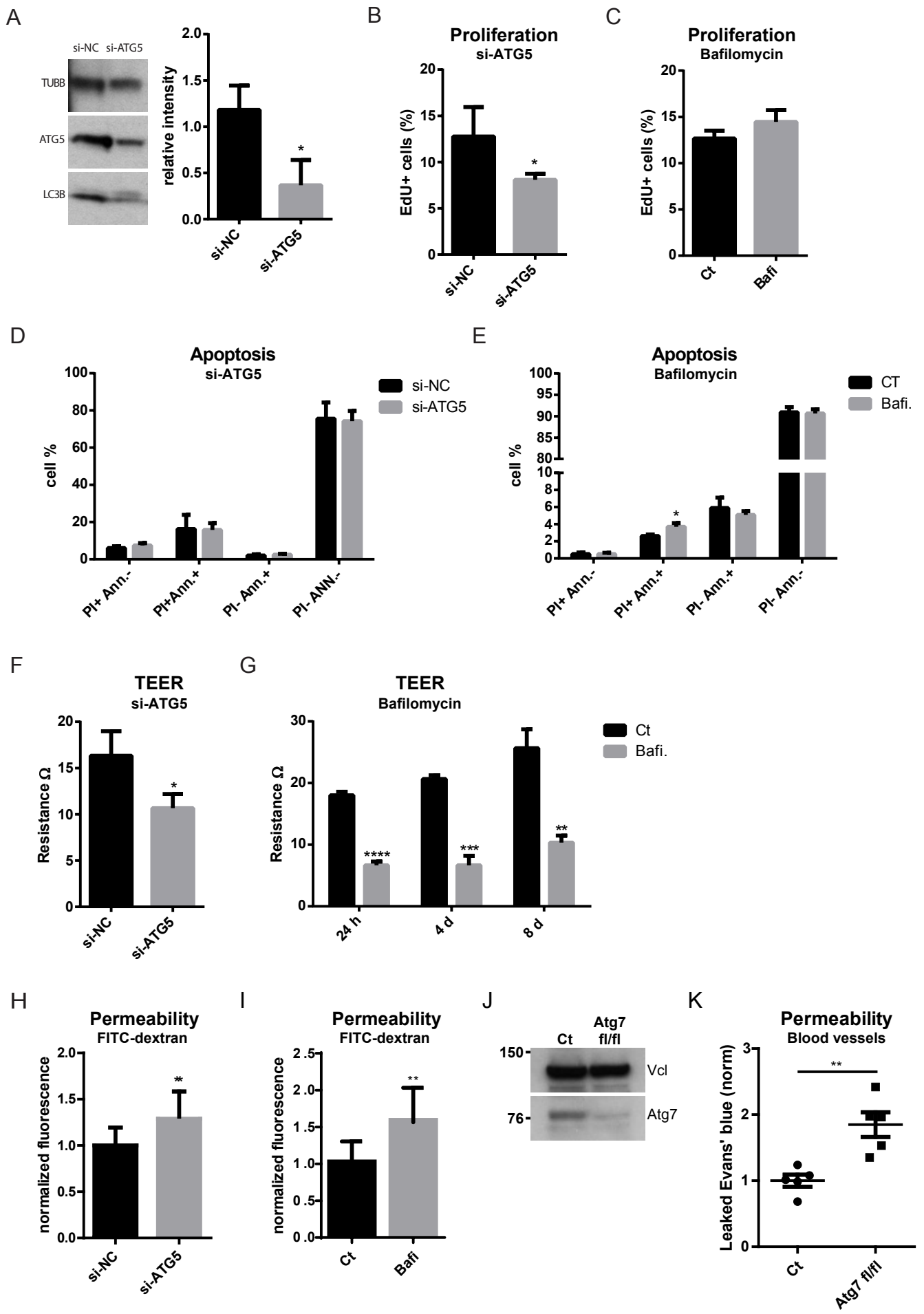
A

Gene names	4d BAFI vs 4d DMSO	SD
APP	1.0405	0.3871
GJA1	0.8476	0.0910
IL6ST	0.8248	0.1795
FHOD1	0.7987	1.0811
SQSTM1	0.7642	0.5557
CRIM1	0.7206	0.2279
CD55;DAF	0.6496	0.7921
JAK1	0.6351	0.4495
PSAP	0.6335	0.3135
MMP14	0.6296	0.1179
TMEM30A	0.5526	0.2082
SLC38A2	0.5498	0.2560
NRP1	0.5126	0.2353
CD81	0.5057	0.4297
B2M	0.4947	0.4426

Gene names	4d BAFI vs 4d DMSO	SD
PPT1	-2.1983	0.1729
CTSB	-1.8161	0.1314
TPP1	-1.7345	0.0998
CTSA	-1.3144	0.2982
UAP1L1	-0.8194	1.2450
CTSZ	-0.7535	0.3370
CSTF3	-0.6394	0.7419
GLB1	-0.6269	0.2059
ITGA2	-0.6162	1.1088
DUSP3	-0.6030	0.6497
CTSC	-0.5727	0.6213
NUCB1	-0.5696	0.2511
KRT18	-0.5554	0.5541
MPRIP	-0.5461	0.2839
SULT1E1	-0.5074	0.6127

B

Gene names	si-ATG5 vs si-NC	SD
TAGLN	2.0007	0.2275
TGFB2	1.3358	0.4121
ALDH1A1	1.2263	0.2599
PTGS2	1.1474	0.4739
PLA2G4C	1.1167	0.1238
BMP1	1.1141	0.3995
RELB	1.0999	0.3678
FABP4	0.9845	0.3196
TNFSF4	0.9325	0.2508
MMP2	0.9174	0.2204
DPYSL4	0.9170	0.2593
FN1	0.8609	0.1359
MMP1	0.8596	0.2195
COL4A1	0.8576	0.5980
COL12A1	0.8562	0.1999

Gene names	si-ATG5 vs si-NC	SD
UHRF1BP1	-2.1638	1.1195
IPPK	-2.0385	0.8934
TFB1M	-1.5909	0.9517
DUS3L	-1.5845	1.9065
KIF14	-1.5361	0.9782
IL1RL1	-1.3688	0.4280
ATG16L1	-1.3247	0.2046
CLDN5	-1.2626	0.3482
MED1	-1.1434	0.2293
EIF4EBP1	-1.1283	0.4788
CCDC56	-1.1244	0.9382
FLNB	-1.0805	0.8160
SMAGP	-1.0770	0.2295
P06733-2	-0.9754	0.0632
BIN1	-0.9247	0.3207

C
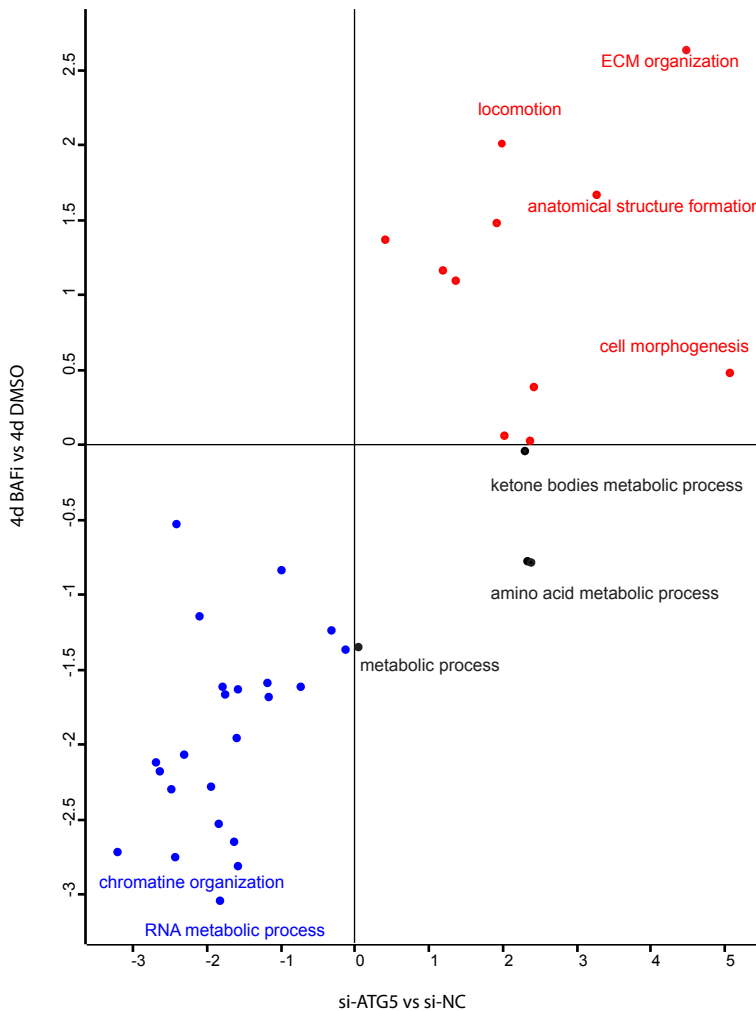
D
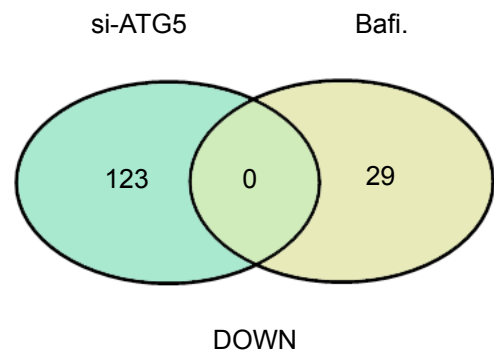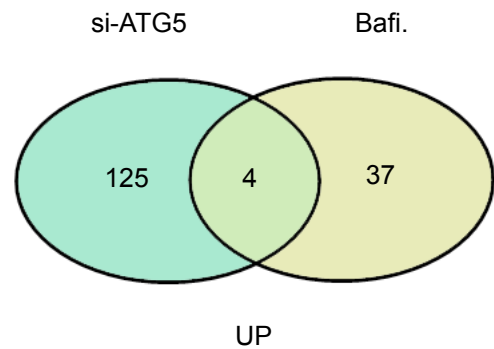
E

| Proteins up-regulated in si-ATG5 and 4h BAFI	
Protein name	Gene names
Complement decay accelerating factor	CD55
Cys-rich motoneuron 1 protein	CRIM1
Endothelial cell-specific molecule 1	ESM1
Rho-related GTP-binding protein RhoB	RHOB

A

| Upstream regulators	Activation z-score		-log(p-value)	
	si-ATG5 vs si-NC	4d Bafi vs 4dDMSO	si-ATG5 vs si-NC	4d Bafi vs 4dDMSO
TGFB1	2.2872	1.7203	7.9138	1.4132
IL1B	1.5375	2.0572	6.8569	5.8206
TP53	1.4051	2.1014	14.3846	4.2281
MYC	-1.9865	1.5086	7.8838	3.6273
genistein	-2.4262	-1.0000	2.3878	7.4605
hydrogen peroxide	1.7341	1.4318	3.0191	4.2466
dexamethasone	1.2176	1.9412	10.6236	2.0324
lipopolysaccharide	2.9670	-0.1489	10.1792	2.8588
EDN1	2.8505	0.2249	5.0362	2.5139
tretinoin	2.2303	0.7484	6.0427	4.7774
D-glucose	2.5803	-0.3906	2.8383	2.3047
PDGF BB	0.8739	1.9640	7.0983	1.7706
MYCN	-1.9322	-0.8083	5.5656	3.9757
PPARG	-0.9430	-1.7321	4.9348	1.4173
IL1	1.4719	1.1879	1.9816	2.4421
TNF	1.7528	0.8959	6.1062	7.5474

B
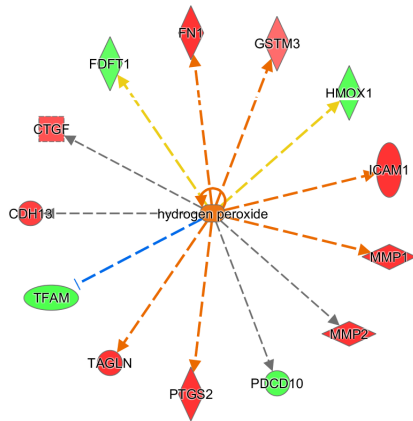
C
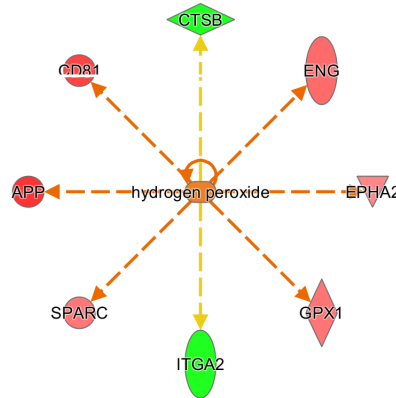
D
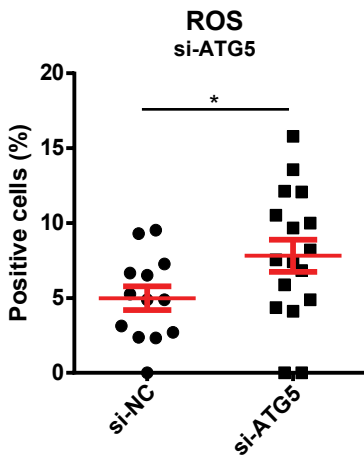
ROS
si-ATG5

E
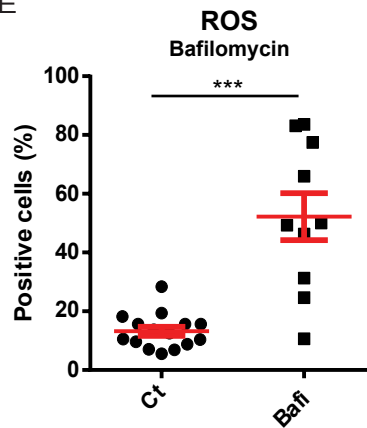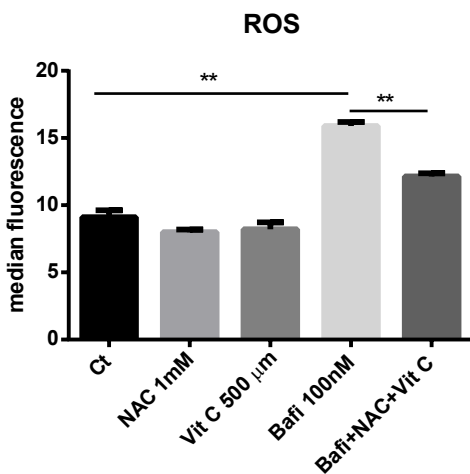

ROS
Bafilomycin

F

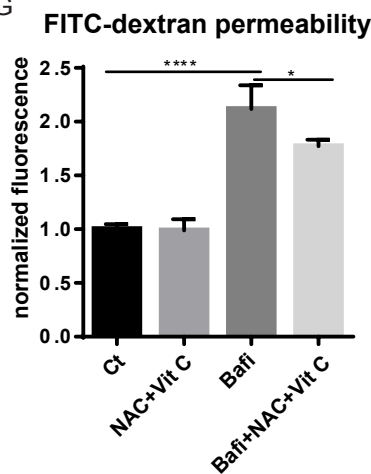

ROS

G

FITC-dextran permeability

In-depth proteomics identifies a role for autophagy in controlling ROS-mediated endothelial permeability

Francesca Patella[1], Lisa J Neilson[1], Dimitris Athineos[1], Zahra Erami[1], Kurt Anderson[1], Karen Blyth[1], Kevin M Ryan[1] and Sara Zanivan[1,*]

[1]Cancer Research UK Beatson Institute, Glasgow G611BD, UK

Supporting Information

Table S1. Proteins identified and quantified in HUVECs (total lysate) forming a tightly confluent monolayer.

Table S2. Gene Ontology (GO) category enrichment analysis of proteins regulated when HUVECs form a tightly confluent monolayer

Table S3. Proteins identified and quantified in HUVECs (total lysate) cultured confluent for 4 days upon 4h bafilomycin treatment.
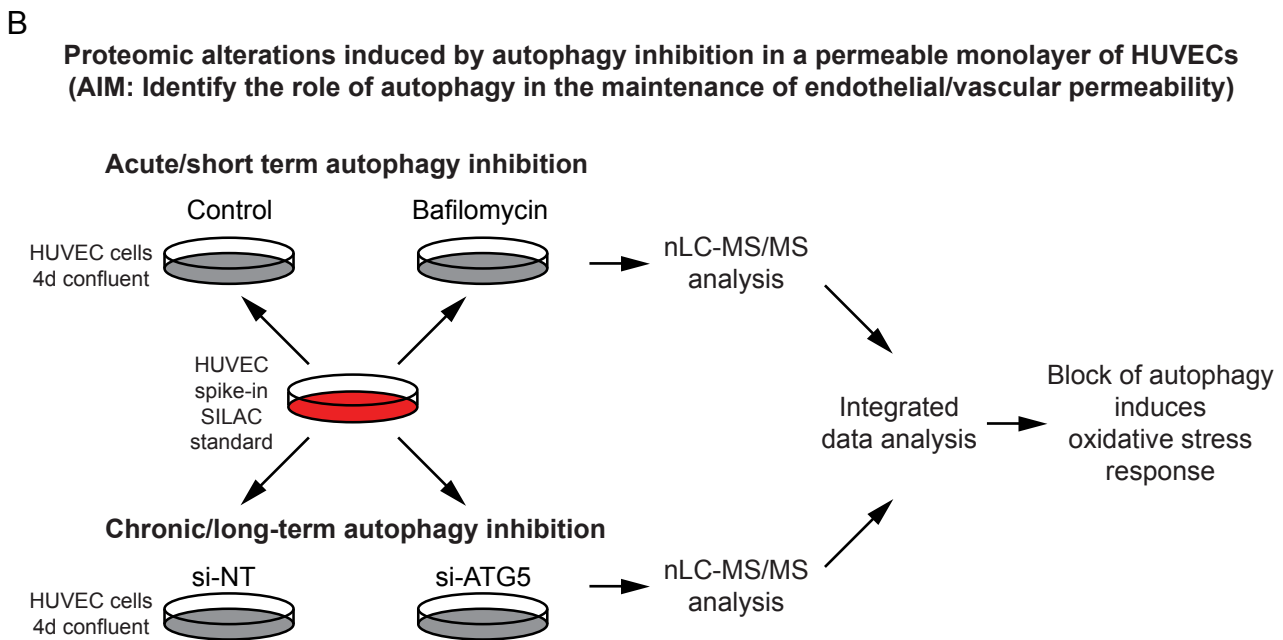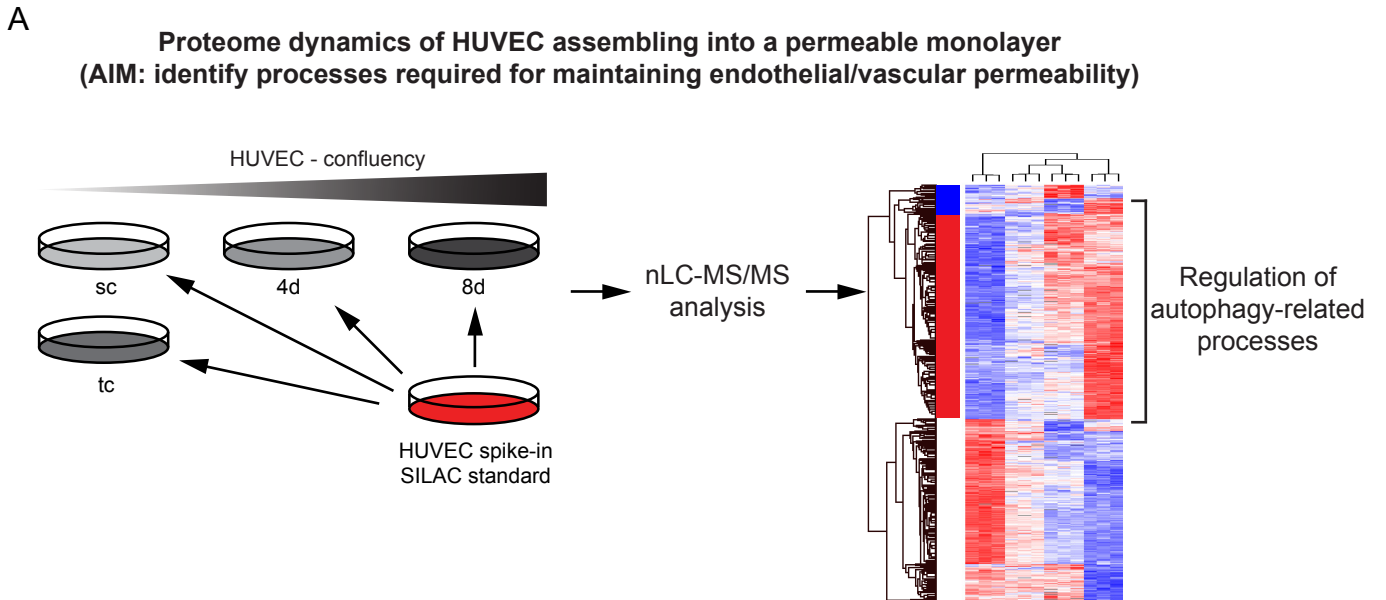
Table S4. Proteins identified and quantified in HUVECs (serum-free conditioned medium) cultured confluent for 4 days upon 4h bafilomycin treatment.

Table S5. Proteins identified and quantified in HUVECs (total lysate) silenced for ATG5.

Table S6. Two dimension (2D) Gene Ontology (GO) category enrichment analysis upon autophagy inhibition with si-ATG5 or bafilomycin.
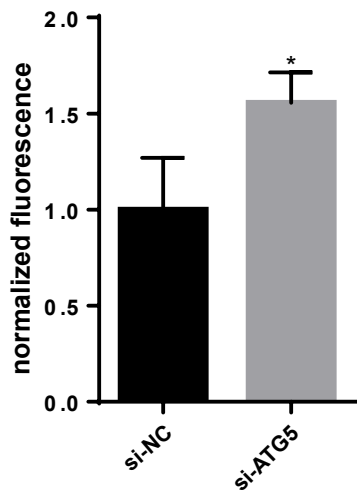
Figure S1. Proteomic analyses. (A) Time resolved SILAC-based proteomic analysis used to identify cellular processes regulated in HUVEC while assembling into a physiologically permeable monolayer. (B) SILAC-based proteomic analysis used to identify proteomic alterations which occur in HUVEC upon acute/short term or chronic/long term inhibition of autophagy. Short term inhibition was triggered by 4h bafilomycin treatment while long term inhibition (4 days) by silencing ATG5 (si-ATG5). Control = DMSO-treated cells; siNT = non targeting siRNA.

Figure S2. Autophagy inhibition increases the permeability of EC monolayer. (A-B) Endothelial cell barrier functionality measured by FITC-albumin permeability upon ATG5 siRNA (A) or bafilomycin (bafi) treatment (B). (C) Increased FITC-albumin permeability due to autophagy blockade by bafilomycin is rescued by scavenging the ROS with NAC and vitamin C (NAC + Vit C).
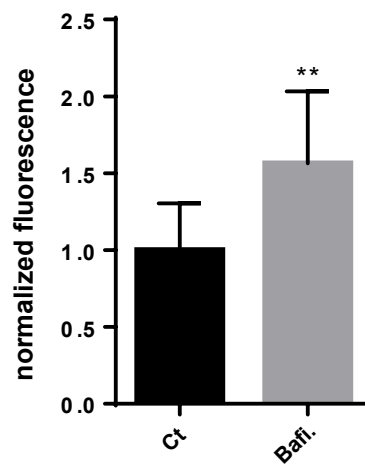
A

**Proteome dynamics of HUVEC assembling into a permeable monolayer
(AIM: identify processes required for maintaining endothelial/vascular permeability)**

B

**Proteomic alterations induced by autophagy inhibition in a permeable monolayer of HUVECs
(AIM: Identify the role of autophagy in the maintenance of endothelial/vascular permeability)**

A

FITC-albumin permeability

B

FITC-albumin permeability

C

FITC-albumin permeability